Diamond & Related Materials xxx (xxxx) 110566

Contents lists available at ScienceDirect

Diamond & Related Materials

journal homepage: www.elsevier.com/locate/diamond

The potential of 2D carbon nitride monolayer as an efficient adsorbent for capturing mercury: A DFT study

Mohamed J. Saadh [a, b], Durgesh Singh [c, 1, **], Diego Mayorga [d], Anjan Kumar [e], María Albuja [f], Ahmad Ismael Saber [g], Mohammed Ahmed Mustafa [h], Yasser Elmasry [i], Noubu Sun [j, *]

[a] Faculty of Pharmacy, Middle East University, Amman 11831, Jordan
[b] Applied Science Research Center, Applied Science Private University, Amman, Jordan
[c] Department of Chemistry, Dr. Harisingh Gour Vishwavidyalaya (A Central University), Sagar, India
[d] Facultad de Mecánica, Escuela Superior Politécnica de Chimborazo (ESPOCH), Riobamba 060155, Ecuador
[e] Department of Electronics and communication Engineering, GLA University, Mathura 281406, India
[f] Facultad de Mecánica, Escuela Superior Politécnica de Chimborazo (ESPOCH), Riobamba 060155, Ecuador
[g] Department of Dentistry, Al-Noor University College, Nineveh, Iraq
[h] Department of Medical Laboratory Techniques University of Imam Jafar Al-Sadiq, College of Technology, Iraq
[i] Department of Mathematics, Faculty of Science, King Khalid University, P.O. Box 9004, Abha 61466, Saudi Arabia
[j] College of Biology and Environmental Engineering, Zhejiang Shuren University, Hangzhou 310015, China

ARTICLE INFO

Keywords:
C_3N monolayer
Mercury
Adsorption
Recovery time
And charge transport

ABSTRACT

Owing to its large surface area and the close similarity between nitrogen and mercury (Hg) in C_3N, two-dimensional C_3N monolayer has the potential of controlling the release of gaseous Hg^0. Using density functional theory (DFT), we investigated the adsorption and conversion mechanism of Hg species on this monolayer surface. The findings demonstrated that C_4N_2 site on the surface of the C_3N monolayer is more capable of adsorbing Hg^0 than C_6 site. Also, the recovery time of the C_3N monolayer for Hg^0 was approximately 17.63 s and 3.49 μs at 298 and 400 K, respectively. The analyses of electronic structure, charge transport, geometric structure, and adsorption stability demonstrated that the C_3N monolayer is an encouraging material for Hg^0 adsorption. The C_3N monolayer could adsorb the oxidizing species of mercury (namely HgBr, HgCl, HgS, and HgO,) more easily than Hg^0, with higher adsorption energy. Overall, the C_3N monolayer is a promising sorbent material, which is capable of controlling gaseous mercury in an efficient way.

1. Introductions

Mercury (Hg) is one of the toxic elements which is released into the water, soil and atmosphere. Also, Hg is accumulated in the food chain, thereby entering the human body. This can present serious threats to ecological environments as well as the human body [1–9]. In 2011, the United States Environmental Protection Agency (EPA) issued the Mercury and Air Toxicity Standard (MATS) with the purpose of reducing the emissions of Hg from power plants, which was implemented in 2012 [10]. China's 12th National People's Congress Standing Committee took a decision in April 2016 on ratifying the Minamata Convention on Hg, urging countries to stop producing, importing and exporting products which contain Hg for protecting the environment and human health.

Combustion of fossil fuels, especially combustion of coal, is one of the main sources of anthropogenic Hg emission to the atmosphere [11–19]. Wet flue gas desulfurization, fabric filters and electrostatic precipitators can be utilized for removing various Hg forms such as Hg^{+1} and Hg^{+2} [20–25]. Nonetheless, owing to its insolubility in water, low melting point and high equilibrium vapor pressure, removing Hg^0 is very difficult via air pollution control devices [26–29]. Therefore, one of the main research directions in novel mercury removal technology is to devise an efficient method for removing Hg^0. In order to remove Hg^0 from flue gas, numerous related removal techniques have been developed. These techniques are based on catalysis [30], ad-

* Corresponding author.
** Corresponding author
E-mail addresses: durgesh.phdchem16@gmail.com (D. Singh), srsunnabo@gmail.com (N. Sun).
[1] Co-corresponding.

https://doi.org/10.1016/j.diamond.2023.110566
Received 25 June 2023; Received in revised form 22 September 2023; Accepted 30 October 2023
0925-9635/© 20XX

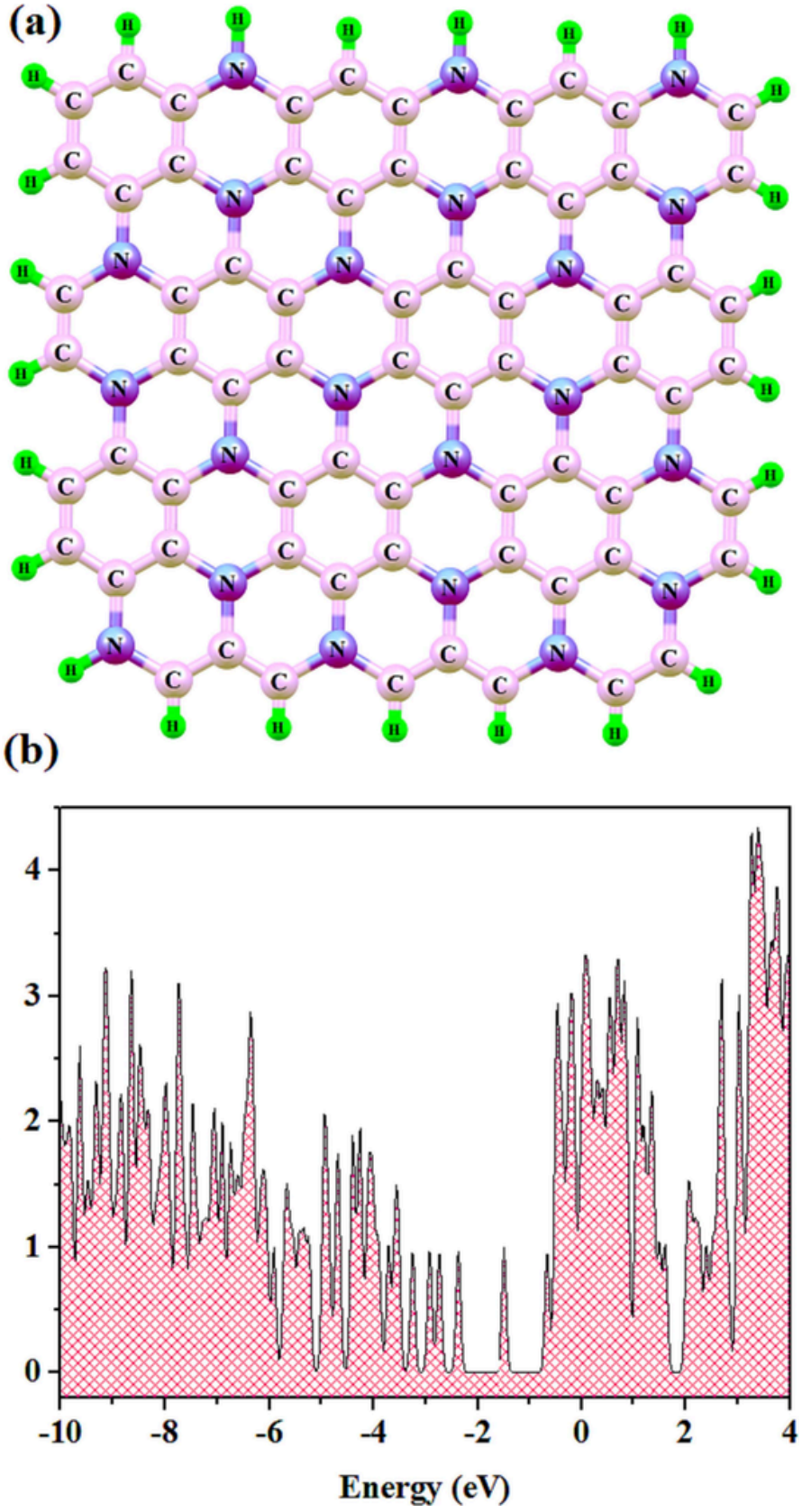

Fig. 1. (a) Optimized structure (top views) and (b) DOS plot of C_3N monolayer.

Table 1
The energy and distance of adsorption and Hg^0 Hirshfeld charges at different sites of C_3N monolayers.

Sites	E_{ads} (kJ/mol)	Hirshfeld charge (e)	distances (Å)
C_6- ring	−19.69	0.109	3.359
C_4N_2-ring	−39.84	0.617	2.933

sorption [31–37] and oxidation [38–45]. Since common adsorbents (mineral adsorbents, calcium-based adsorbents, activated carbon, and fly ash) have limitations such as secondary Hg pollution, low efficiency, and high cost, researchers have turned their attention to Hg^0 removal by means of carbon-heteroatom-containing adsorbents [46–51]. We can obtain good adsorption rate and capacity by using carbon-heteroatom-containing adsorbents, which can be efficiently used for Hg removal [52,53].

These days, one of the emerging novel semi-conductors with indirect bandgap (BG) is a two-dimensional (2D) material called C_3N monolayer, which has carbon and nitrogen atoms [46–49,51,54–57]. By replacing 2 atoms of N onto a 2 × 2 supercell of graphene (Gr), we can produce an intrinsic C_3N monolayer with 6C atoms and 2 N atoms, which exhibits a planar honeycomb lattice (PHL) with 4.9 Å lattice constant [58]. Replacing N atoms provides the C_3N monolayer with higher carrier mobility and stronger chemical activity compared to Gr, but structural stability remains the same [59]. The above-mentioned characteristics of the C_3N monolayer make it possible to use it as a promising sensing material in nanoscale devices. As mentioned above, the PHL of the C_3N monolayer, which is similar to Gr, provides this material with unique characteristics, including high conductivity, microporous structure, surface area, and unique mechanical characteristics [59], which are essential to a good adsorption material for removing Hg.

Within this study, we scrutinized the adsorption and removal behavior associated with elemental mercury (Hg^0) on the 2D C_3N monolayer using DFT calculations and by performing analyses related to reaction energy barrier, charge transport, atomic orbital energy of adsorption, and BG. In order to clarify the removal mechanism of Hg^0 on the C_3N monolayer, we took the most probable Hg^0 transformation path. In general, the current study provides new insights into removing Hg^0 using the 2D C_3N monolayer to guide researchers on designing sorbents. The results of this study can guide future research on designing sorbents for the removal of mercury from flue gas, helping to reduce mercury emissions and protect human and environmental health.

2. Computational details

The calculations were performed using GAMESS software program with 6–31 + + G** (d) basis set with the functional Perdew-Burke-Ernzerhof (PBE) [60–65]. For evaluating interactions with long-range and Van der Waals forces have been used DFT-D Grimme's term [66]. Also, the displacement, maximum force, and the energy tolerance accuracy were set to 5 × 10^{-3} Å, 2 × 10^{-3} Ha/Å and 10^{-5} Ha respectively [67–71]. Also, smearing, the global orbital cut-off radius, and self-consistent loop energy were set to 0.005 Ha, 5.0 Å, and 10^{-6} Ha, respectively, for computations of static electronic structure for ensuring the correctness of the total energy results [72–75]. Have been performed the Hirshfeld analysis for analyzing the molecular and atomic charge in the systems under study. The charge transport for the adsorption of Hg^0 computing the entire charges of particular molecules which were adsorbed have been defined. A negative and positive charge transport shows the electron acceptor and donor nature of the Hg^0 molecule respectively. For charge transport in Hg^0 adsorption systems, the Mullikan method was used for comparing the results with those of the Hirshfeld method [76].

The energy of adsorption, designated by E_{ads}, is one of the significant criteria for investigating the adsorption process mechanism. The process for the adsorption of molecule X on surface of solid Y is exothermic in nature. E_{ads} as follows below:

$$E_{ads} = E_{XY} - (E_X + E_Y) \quad (1)$$

where E_{ads} = adsorption energy; E_{XY} = total energy after the adsorption of molecule X adsorbed on the surface of solid Y. E_X and E_Y = total energy of molecule X and solid adsorbent Y in the ground state. There are two types of adsorption processes, namely physisorption or physical adsorption with E_{ads} of less than −50 kJ/mol and chemisorption or chemical adsorption with E_{ads} of more than −50 kJ/mol.

The difference in electron density ($\Delta\rho$) have been calculated as follows:

$$\Delta\rho = \rho_{XY} - \rho_X - \rho_Y \quad (2)$$

whereρ_{XY} = total electron density of the adsorption system. ρ_X = unperturbed electron densities of surface X; and ρ_Y = isolated adsorbate molecule Y.

3. Results and discussion

3.1. Structure and the electronic parameters of the C_3N monolayer

According to Fig. 1(a), the C_3N monolayer includes a PHL with six C atoms and 2 N atoms. In this monolayer, σ and π bonds are formed by the sp^2 hybridization of C and N atomic orbitals. The length of C—C and C—N bonds are 1.42 Å and 1.401 Å respectively, in line with values reported in the literature [77]. As illustrated in Fig. 1 b, we selected an orthogonal C_3N monolayer with a BG of 0.89 eV, in line with the value reported in the literature [77]. The density of states (DOS) plot of pristine C_3N monolayer demonstrates the peaks of fermi level at −1.96 eV. We conducted the Bader charge analysis for computing the charge transport [78]. In fact, each N atom received 1.26 e electrons from its adjacent C atoms because the electronegativity of N (3.04) is more than that of C (2.55) (Table 1).

3.2. Hg^0 adsorption on the C_3N monolayer

One of the important steps in the conversion of heterogeneous Hg is the adsorption of Hg^0 on the surface of the C_3N monolayer. Therefore, first investigated the adsorption behavior of Hg^0 on the C_3N monolayer. As illustrated in Fig. 2, there were two possible sites for the adsorption of Hg^0 on the surface of the C_3N monolayer. Hg^0 was adsorbed at the N atom of the C_4N_2 ring site with higher E_{ads} of −39.84 kJ/mol than that of the C atom of C_6 ring site with E_{ads} of −19.69 kJ/mol. Additionally, at C_4N_2 site, the distance between Hg atom and N atom was 2.933 Å, which was shorter than that between Hg atom and the C atom at C_6 site that was 3.359 Å. Based on the results, Hg atom had a physical adsorption at C_6 site, but it had a strong physical adsorption at C_4N_2 site on the surface of the C_3N monolayer. In the substituted C_4N_2 ring, a bond between Hg and the remaining N was formed because the other N is absent, which was capable of facilitating the adsorption of Hg atom. As illustrated in Fig. 3, have been performed the analysis of charge density difference to further assess the charge transport in the stable adsorption system. Based on the results, there was a charge redistribution in the adsorption of Hg^0 on the C_3N monolayer surface. In general, there was an accumulation of electrons near the C atom and there was a depletion of electrons near Hg and N atoms. The considerable transport of electrons confirmed that the Hg atom and N atom interacted at C_4N_2 site. Based on the Hirshfeld analysis [79], the amount of electron transport for Hg was more at C_4N_2 site (0.617 e) than the amount of electron transport at C_6 site (0.109 e). Overall, the findings demonstrated that the efficiency of C_4N_2 site is more than that of C_6 site in adsorbing Hg. The value of adsorption energy reported in the literature for other com-

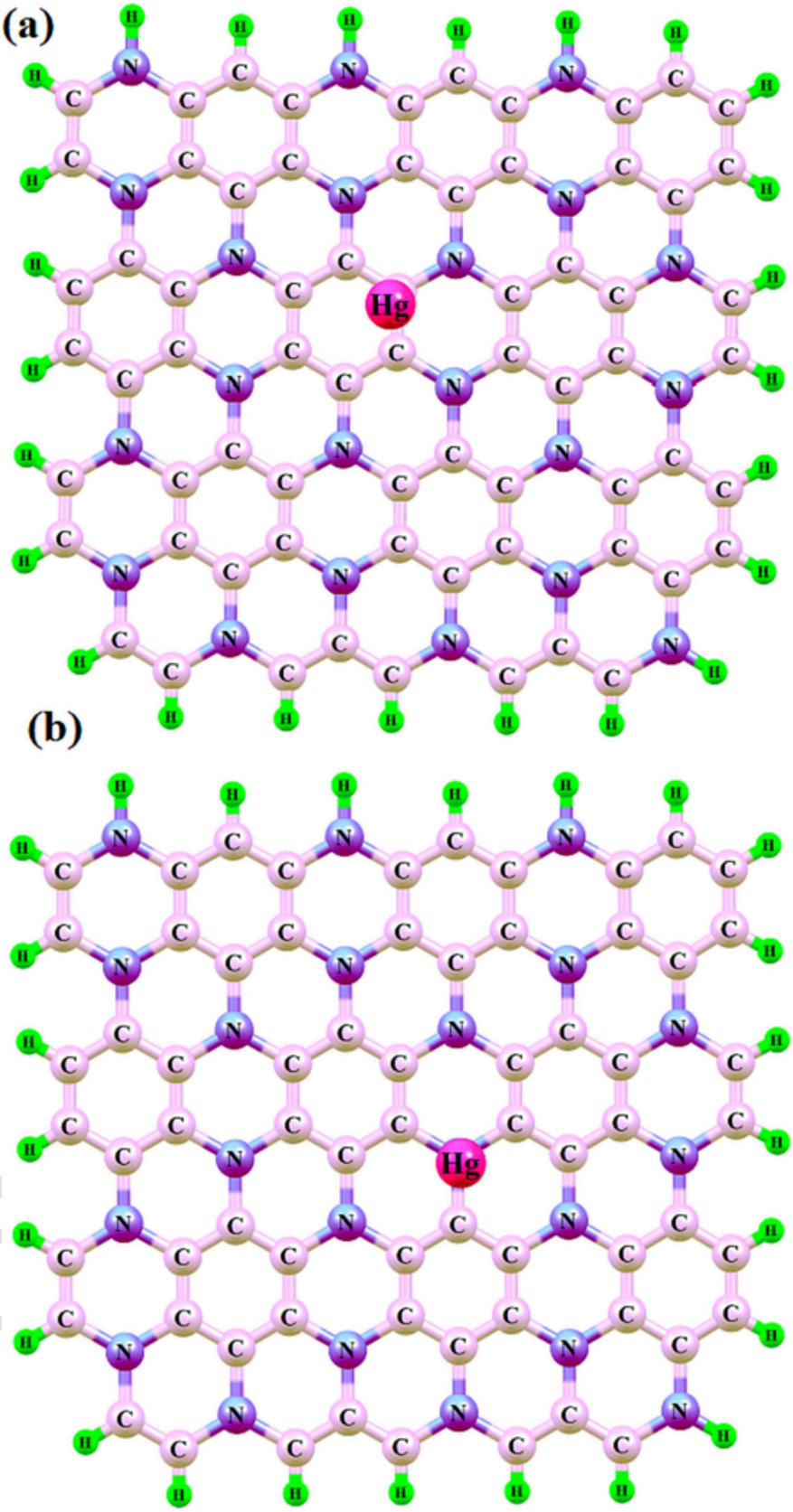

Fig. 2. Optimized structures for adsorption of Hg^0 at sites (a) C_6 and (b) C_4N_2 on the C_3N surface.

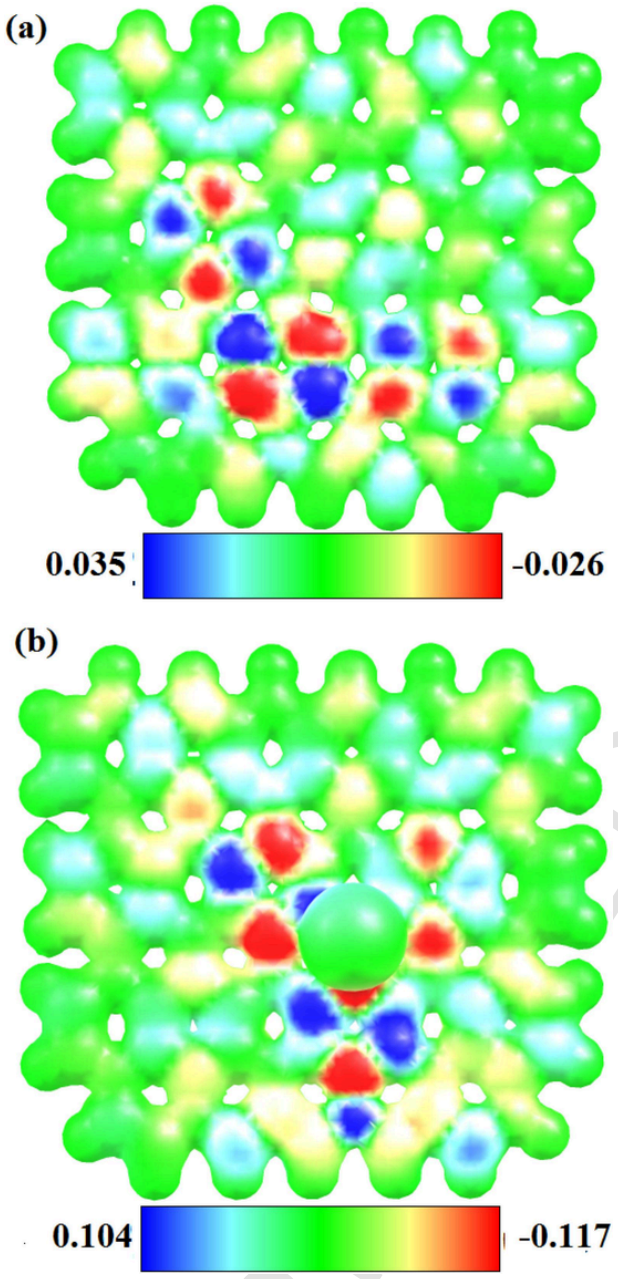

Fig. 3. Map of the charge density difference for the C_3N monolayer (a) before and (b) after adsorption of Hg^0.

pounds on the C_3N surface shows that the Hg absorption energy is higher than carbon dioxide [80], nitrogen dioxide, and sulfur dioxide [81].

3.3. Electronic characteristics

Using the DOS diagrams in Fig. 4, which was plotted after the adsorption, the interaction mechanism between the Hg^0 atoms at C_4N_2 site on the surface of the C_3N monolayer have been understand. Fig. 4 depicts the DOS diagrams of the C_3N monolayer after the adsorption of the Hg^0 molecule. Due to the charge transport from Hg^0 to the surface of the C_3N monolayer, all the orbitals of Hg^0 atom moved to levels with low energy after Hg^0 was adsorbed on the surface of the C_3N monolayer. At C_4N_2 sites, the hybridization of N atom can be observed in the s- / p orbitals between Hg^0 and the neighboring N atom close to the Fermi level (−1.78 eV). In agreement with previous results, a strong orbital hybridization resulted in a strong interaction for the Hg^0 adsorption on the monolayer surface.

Also was investigated the BG to expound on the difference between the two adsorption sites. The BG of the pristine C_3N monolayer was 0.89 eV, demonstrating that the energy needed to transport electrons to the conduction band (CB) from the valence band (VB) was low. Also, following the adsorption of Hg^0 on the monolayer surface, BG decreased from 0.89 eV to 0.65 eV. The adsorption of Hg^0 at C_4N_2 site resulted in a significant decrease in the BG, facilitating the transport of electrons from the VB to the CB. These results can be used as a signal for the adsorption of Hg^0.

3.4. Evaluation of C_3N monolayer recovery time (RT)

As discussed above, the C_3N monolayer is a good adsorbent for Hg^0 due to its significant adsorption energy. However, the reusable characteristic of the C_3N monolayer should also be taken into account in order to consider the C_3N monolayer as a good adsorbent, which can be assessed by the RT. The RT in keeping with the transition state theory as follows [82]:

$$\tau = \upsilon_0^{-1} \exp\left(\frac{-E_{ads}}{k_B T}\right) \quad (3)$$

where υ_0 = attempt frequency (10^{-13} s^{-1}); and E_{ads} = adsorption energy [83]. Here, kB = Boltzmann constant; and T = temperature (K). At ambient temperature (298 K), the RT for the desorption of Hg^0 from the surface of the C_3N adsorbent was 17.63 μs. Moreover, at higher temperature than 298 K, i.e., 400 K, the RT was computed to be 3.49 μs on the C_3N monolayer, demonstrating the reusable characteristic of the C_3N monolayer under humid conditions and/or at higher temperatures than 298 K. Therefore, due to its excellent stability and short RT, have been considered the C_3N monolayer a promising Hg^0 adsorbent.

3.5. Adsorption of various Hg species on the C_3N monolayer

The Hg removal mechanism is dependent on the Hg species which exists in industrial flue gas. Hence, explaining the adsorption behavior of different species of Hg is of paramount importance in gaining a deeper understanding of its conversion mechanism. There are two important types of oxidized species of Hg, namely mercury sulfide (HgS) and mercury oxide (HgO). However, two important intermediate materials in the Hg conversion process are HgBr and HgCl [34]. Therefore, for further investigated how the adsorption ability of the C_3N monolayer (defective and clean) was affected by different species of Hg such as HgBr, HgCl, HgS, HgO, and Hg^0. Fig. 5 and Fig. 1S shows the obtained E_{ads} on the surface of the C_3N monolayer. Each Hg species has a different E_{ads} on the C_3N monolayer surface, which shows that there is a difference in the bonding strength between different Hg species and the C_3N monolayer. Overall, E_{ads} of the different species of Hg is in the following order: HgCl > HgBr > HgS > HgO > Hg^0 This show that the C_3N monolayer can capture Hg in its oxidation form more easily. Strong physical adsorption is the main cause for the adsorption of different species of Hg on the C_3N monolayer rather than physisorption (or Van der Waals force). Furthermore, the charge transport in the Hg atom of HgO (0.873 e), HgCl (0.664 e) and HgBr (0.703 e) was more, demonstrating the strong physical adsorption of oxidized species of Hg on the surface of the C_3N monolayer.

4. Conclusion

Using DFT, the adsorption and conversion mechanism of Hg^0 on the 2D C_3N monolayer was investigated and expounded on. Based on the findings, Hg^0 had a physical adsorption at C_6 site, while it had a strong physical adsorption at C_4N_2 site on the surface of this monolayer. Obvi-

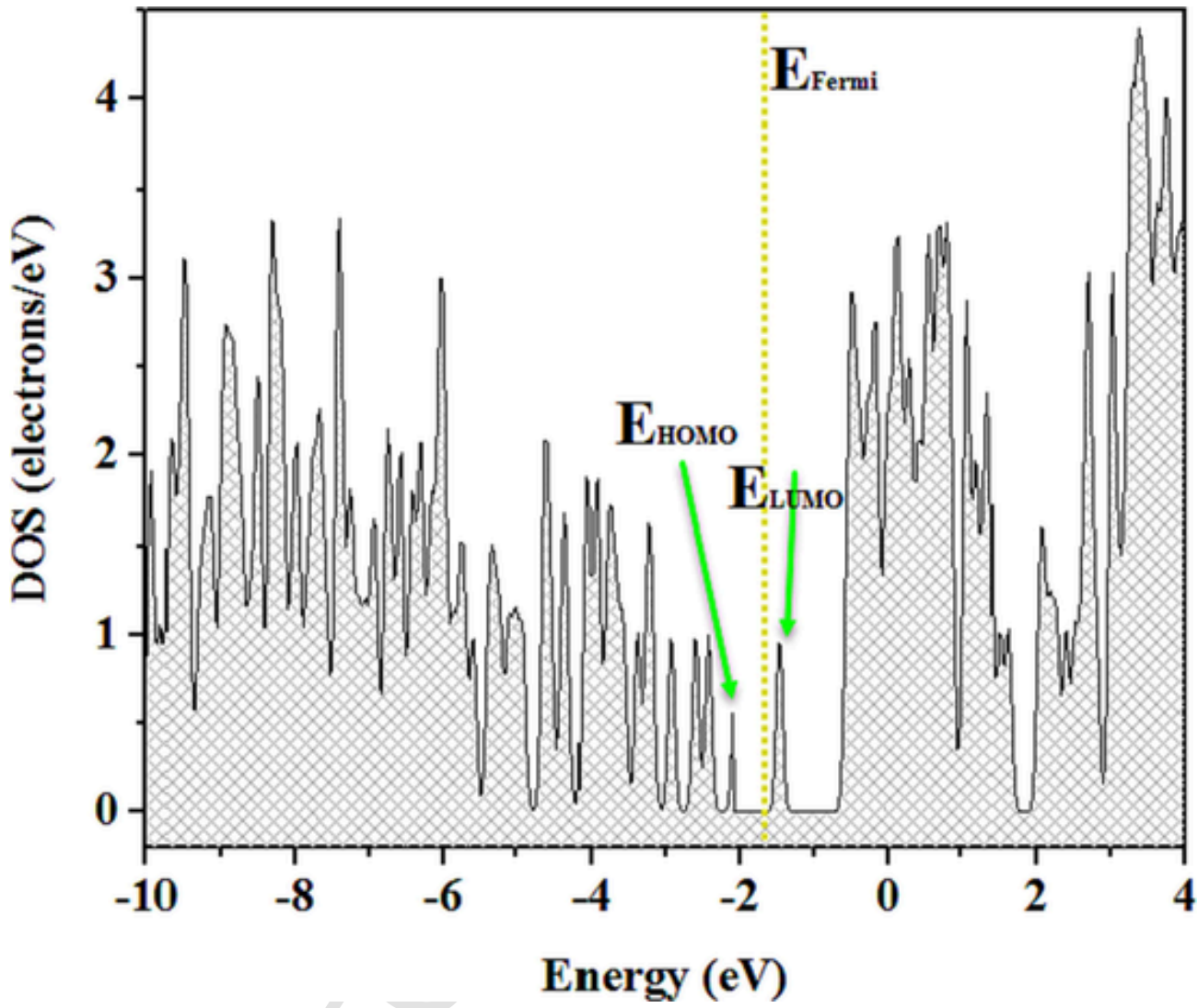

Fig. 4. DOS plot of C_3N monolayer after adsorption Hg^0 (the dash line is Fermi level).

ously, the considerable charge transport and orbital hybridization resulted in a strong interaction between Hg^0 and the C_3N monolayer. The RT of the C_3N monolayer for Hg^0 was approximately 17.63 s and 3.49 μs at different temperatures of 298 and 400 K respectively. Therefore, the C_3N monolayer was considered a promising adsorbent material with noticeable recovery performance for Hg^0 adsorption. Also, compared to Hg^0, oxidized Hg species tend to be adsorbed more by the C_3N monolayer with higher E_{ads}. The current work suggests that the C_3N monolayer is a good adsorbent, capable of controlling gaseous Hg in flue gas in an efficient way.

Supplementary data to this article can be found online at https://doi.org/10.1016/j.diamond.2023.110566.

Funding

None.

Ethical approval

Not required.

CRediT authorship contribution statement

M. J. Saadh, D. Singh, D. Mayorga, A. Kumar, M. Albuja, A. I. Saber: Methodology, Software, Writing - review & editing; Management and responsibility for the research activity planning and execution; **M. A. Mustafa:** Conceptualization, Methodology, Software, Writing, Conceptualization, Methodology; **Y. Elmasry, N. Sun**: Writing - original draft, Methodology, Software, review & editing.

Declaration of competing interest

The authors declare that they have no known competing financial interests or personal relationships that could have appeared to influence the work reported in this paper.

Data availability

No data was used for the research described in the article.

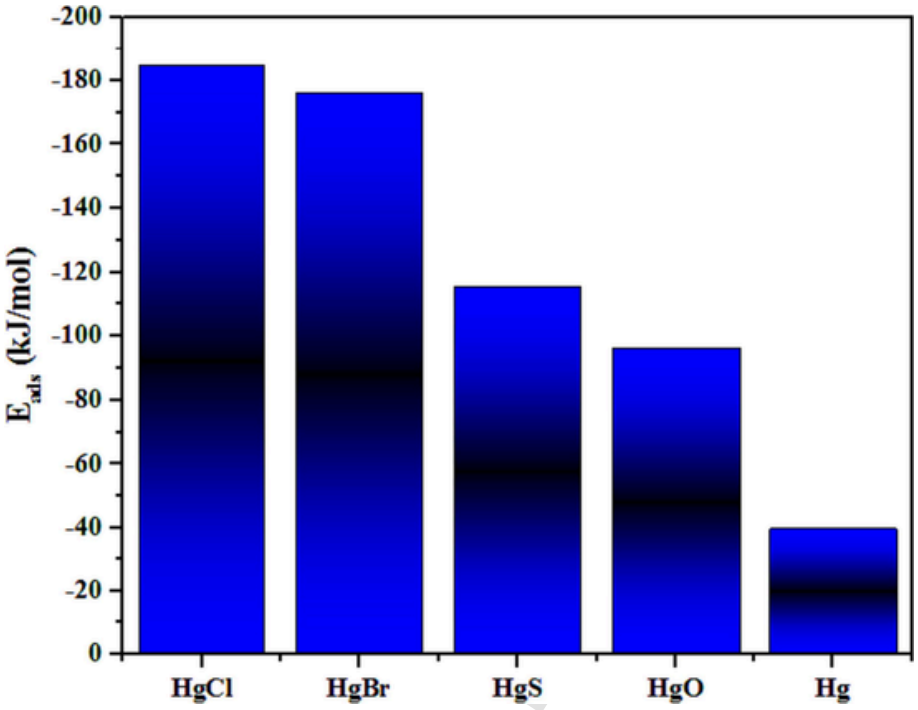

Fig. 5. Comparison of the energy of adsorption for different Hg species on the C_3N monolayer.

Acknowledgments

The authors extend their appreciation to the Deanship of Scientific Research at King Khalid University for funding this work through the Large Groups under grant number (RGP.2/120/44).

References

[1] M. Rallo, M.A. Lopez-Anton, M.L. Contreras, M.M. Maroto-Valer, Mercury policy and regulations for coal-fired power plants, Environ. Sci. Pollut. Res. 19 (2012) 1084–1096.
[2] S. Zhang, Y. Zhao, J. Yang, Y. Zhang, P. Sun, X. Yu, J. Zhang, C. Zheng, Simultaneous NO and mercury removal over MnOx/TiO2 catalyst in different atmospheres, Fuel Process. Technol. 166 (2017) 282–290.
[3] Y. Li, J. Zhang, Y. Zhao, C. Zheng, Volatility and speciation of mercury during pyrolysis and gasification of five Chinese coals, Energy Fuel 25 (2011) 3988–3996.
[4] F. Wang, M.N. Khan, I. Ahmad, H. Ahmad, H. Abu-Zinadah, Y.-M. Chu, Numerical solution of traveling waves in chemical kinetics: time fractional fishers equations, Fractals, 30(2022)2240051.
[5] Z.-Y. He, A. Abbes, H. Jahanshahi, N.D. Alotaibi, Y. Wang, Fractional-order discrete-time SIR epidemic model with vaccination: chaos and complexity, Mathematics 10 (2022) 165.
[6] H. Guan, S. Huang, J. Ding, F. Tian, Q. Xu, J. Zhao, Chemical environment and magnetic moment effects on point defect formations in CoCrNi-based concentrated solid-solution alloys, Acta Mater. 187 (2020) 122–134.
[7] W. Zhu, M. Deng, D. Chen, Z. Zhang, W. Chai, D. Chen, H. Xi, J. Zhang, C. Zhang, Y. Hao, Dual-phase CsPbCl3–Cs4PbCl6 perovskite films for self-powered, visible-blind UV photodetectors with fast response, ACS Appl. Mater. Interfaces 12 (2020) 32961–32969.
[8] S.-X. Mao, J.-Y. Song, W.-S. Zhu, H.-M. Li, J.-Y. Pang, D.-B. Dang, Y. Bai, Heterogeneous oxidative desulfurization of fuels using amphiphilic mesoporous phosphomolybdate-based poly (ionic liquid) over a wide temperature range, Fuel 352 (2023) 128982.
[9] W. Kuang, H. Wang, X. Li, J. Zhang, Q. Zhou, Y. Zhao, Application of the thermodynamic extremal principle to diffusion-controlled phase transformations in Fe-C-X alloys: modeling and applications, Acta Mater. 159 (2018) 16–30.
[10] Z. Zhongming, L. Linong, Z. Wangqiang, L. Wei, Global Mercury Assessment 2013: Sources, Emissions, Releases, and Environmental Transport, 2013.
[11] E.J. Granite, H.W. Pennline, R.A. Hargis, Novel sorbents for mercury removal from flue gas, Ind. Eng. Chem. Res. 39 (2000) 1020–1029.
[12] Y. Yuan, Y. Zhao, H. Li, Y. Li, X. Gao, C. Zheng, J. Zhang, Electrospun metal oxide–TiO2 nanofibers for elemental mercury removal from flue gas, J. Hazard. Mater. 227 (2012) 427–435.
[13] S.N. Hajiseyedazizi, M.E. Samei, J. Alzabut, Y.-m. Chu, On multi-step methods for singular fractional q-integro-differential equations, Open Math. 19 (2021) 1378–1405.
[14] Y.-M. Chu, U. Nazir, M. Sohail, M.M. Selim, J.-R. Lee, Enhancement in thermal energy and solute particles using hybrid nanoparticles by engaging activation energy and chemical reaction over a parabolic surface via finite element approach, Fract. Fraction. 5 (2021) 119.
[15] C. Zhao, M. Xi, J. Huo, C. He, L. Fu, Electro-reduction of N2 on nanostructured materials and the design strategies of advanced catalysts based on descriptors, Mater. Today Phys. 22 (2022) 100609.
[16] Y.-M. Chu, B. Shankaralingappa, B. Gireesha, F. Alzahrani, M.I. Khan, S.U. Khan, Combined impact of Cattaneo-Christov double diffusion and radiative heat flux on bio-convective flow of Maxwell liquid configured by a stretched nano-material surface, Appl. Math. Comput. 419 (2022) 126883.
[17] S. Dong, H. Zhang, D. Yuan, Supramolecular nonwoven materials via thermally induced precursor crystallization of nanocrystalline fibers/belts for recyclable air filters, ACS Appl. Nano Mater.6 (2023)9548-9557.
[18] Z. Guo, R. Zhan, Y. Shi, D. Zhu, J. Pan, C. Yang, Y. Wang, J. Wang, Innovative and green utilization of zinc-bearing dust by hydrogen reduction: recovery of zinc and lead, and synergetic preparation of Fe/C micro-electrolysis materials, Chem. Eng. J. 456 (2023) 141157.
[19] Y. Liu, J. Qin, L. Lu, J. Xu, X. Su, Enhanced microwave absorption property of silver decorated biomass ordered porous carbon composite materials with frequency selective surface incorporation, Int. J. Miner. Metall. Mater. 30 (2023) 525–535.
[20] H. Li, Y. Li, C.-Y. Wu, J. Zhang, Oxidation and capture of elemental mercury over SiO2–TiO2–V2O5 catalysts in simulated low-rank coal combustion flue gas, Chem. Eng. J. 169 (2011) 186–193.
[21] L.-p. Zhong, C. Yan, W.-y. Li, W.-p. Pan, K.-c. Xie, Effect of the existing air pollutant control devices on mercury emission in coal-fired power plants, J. Fuel Chem. Technol. 38 (2010) 641–646.
[22] Y. Wang, Y. Liu, Z. Wu, J. Mo, B. Cheng, Experimental study on the absorption behaviors of gas phase bivalent mercury in Ca-based wet flue gas desulfurization slurry system, J. Hazard. Mater. 183 (2010) 902–907.
[23] M.-K. Wang, M.-Y. Hong, Y.-F. Xu, Z.-H. Shen, Y.-M. Chu, Inequalities for generalized trigonometric and hyperbolic functions with one parameter, J. Math. Inequal. 14 (2020) 1–21.
[24] T.-H. Zhao, Y.-M. Chu, Y.-L. Jiang, Y.-M. Li, Best possible bounds for Neuman-Sándor mean by the identric, quadratic and contraharmonic means, in: Abstract and Applied Analysis, Hindawi, 2013.
[25] Y. Yuan, Z. Li, X. Peng, K. Xue, M. Liu, Z. Fang, L. Wang, H. Du, H. Lu, Functional gel cathode strategy to enhance the long-term cyclability of the lithium-polysulfide full cell, Electrochim. Acta 140052 (2022).
[26] S. Tao, C. Li, X. Fan, G. Zeng, P. Lu, X. Zhang, Q. Wen, W. Zhao, D. Luo, C. Fan, Activated coke impregnated with cerium chloride used for elemental mercury removal from simulated flue gas, Chem. Eng. J. 210 (2012) 547–556.
[27] H. Xu, N. Yan, Z. Qu, W. Liu, J. Mei, W. Huang, S. Zhao, Gaseous heterogeneous catalytic reactions over Mn-based oxides for environmental applications: a critical review, Environ. Sci. Technol. 51 (2017) 8879–8892.
[28] Y.-M. Chu, H. Wang, T.-H. Zhao, Sharp bounds for the Neuman mean in terms of the quadratic and second Seiffert means, J. Inequal. Appl. 2014 (2014) 1–14.
[29] Z. Sun, T. Wang, R. Zhang, H. Li, Y. Wu, S. Toan, Z. Sun, Boosting hydrogen production via deoxygenation-sorption-enhanced biomass gasification, Bioresour.

Technol. 382 (2023) 129197.
[30] J. Yang, Y. Zhao, J. Zhang, C. Zheng, Regenerable cobalt oxide loaded magnetosphere catalyst from fly ash for mercury removal in coal combustion flue gas, Environ. Sci. Technol. 48 (2014) 14837–14843.
[31] H. Liu, J. Yang, C. Tian, Y. Zhao, J. Zhang, Mercury removal from coal combustion flue gas by modified palygorskite adsorbents, Appl. Clay Sci. 147 (2017) 36–43.
[32] J. Yang, Y. Zhao, S. Ma, B. Zhu, J. Zhang, C. Zheng, Mercury removal by magnetic biochar derived from simultaneous activation and magnetization of sawdust, Environ. Sci. Technol. 50 (2016) 12040–12047.
[33] S. Zhang, Y. Zhao, J. Yang, J. Zhang, C. Zheng, Fe-modified MnOx/TiO2 as the SCR catalyst for simultaneous removal of NO and mercury from coal combustion flue gas, Chem. Eng. J. 348 (2018) 618–629.
[34] X. Chen, D. Wang, T. Wang, Z. Yang, X. Zou, P. Wang, W. Luo, Q. Li, L. Liao, W. Hu, Enhanced photoresponsivity of a GaAs nanowire metal-semiconductor-metal photodetector by adjusting the fermi level, ACS Appl. Mater. Interfaces 11 (2019) 33188–33193.
[35] Y. Huang, C. An, Q. Zhang, L. Zang, H. Shao, Y. Liu, Y. Zhang, H. Yuan, C. Wang, Y. Wang, Cost-effective mechanochemical synthesis of highly dispersed supported transition metal catalysts for hydrogen storage, Nano Energy 80 (2021) 105535.
[36] Y. Liu, B. Fan, B. Xu, B. Yang, Ambient-stable polyethyleneimine functionalized Ti3C2Tx nanohybrid corrosion inhibitor for copper in alkaline electrolyte, Mater. Lett. 337 (2023) 133979.
[37] T. Tang, M. Zhou, J. Lv, H. Cheng, H. Wang, D. Qin, G. Hu, X. Liu, Sensitive and selective electrochemical determination of uric acid in urine based on ultrasmall iron oxide nanoparticles decorated urchin-like nitrogen-doped carbon, Colloids Surf. B: Biointerfaces 216 (2022) 112538.
[38] Y. Liu, Y. Wang, Q. Wang, J. Pan, Y. Zhang, J. Zhou, J. Zhang, A study on removal of elemental mercury in flue gas using Fenton solution, J. Hazard. Mater. 292 (2015) 164–172.
[39] F. Zhan, C. Li, G. Zeng, S. Tao, Y. Xiao, X. Zhang, L. Zhao, J. Zhang, J. Ma, Experimental study on oxidation of elemental mercury by UV/Fenton system, Chem. Eng. J. 232 (2013) 81–88.
[40] T.-H. Zhao, Z.-H. Yang, Y.-M. Chu, Monotonicity properties of a function involving the psi function with applications, J. Inequal. Appl. 2015 (2015) 1–10.
[41] Y.-M. Chu, T.-H. Zhao, Convexity and concavity of the complete elliptic integrals with respect to Lehmer mean, J. Inequal. Appl. 2015 (2015) 1–6.
[42] H. He, Q.-Q. Zhu, Y. Yan, H.-W. Zhang, Z.-Y. Han, H. Sun, J. Chen, C.-P. Li, Z. Zhang, M. Du, Metal–organic framework supported Au nanoparticles with organosilicone coating for high-efficiency electrocatalytic N2 reduction to NH3, Appl. Catal. B Environ. 302 (2022) 120840.
[43] S. Mu, Q. Liu, P. Kidkhunthod, X. Zhou, W. Wang, Y. Tang, Molecular grafting towards high-fraction active nanodots implanted in N-doped carbon for sodium dual-ion batteries, Natl. Sci. Rev. 8 (2021) nwaa178.
[44] Y. Zhao, B. Zhang, H. Hou, W. Chen, M. Wang, Phase-field simulation for the evolution of solid/liquid interface front in directional solidification process, J. Mater. Sci. Technol. 35 (2019) 1044–1052.
[45] Z. Liu, B. Fan, J. Zhao, B. Yang, X. Zheng, Benzothiazole derivatives-based supramolecular assemblies as efficient corrosion inhibitors for copper in artificial seawater: formation, interfacial release and protective mechanisms, Corros. Sci. 212 (2023) 110957.
[46] D. Ma, J. Zhang, Y. Tang, Z. Fu, Z. Yang, Z. Lu, Repairing single and double atomic vacancies in a C 3 N monolayer with CO or NO molecules: a first-principles study, Phys. Chem. Chem. Phys. 20 (2018) 13517–13527.
[47] H. Wang, H. Wu, J. Yang, C3N: a two dimensional semiconductor material with high stiffness, superior stability and bending Poisson's effect, in: arXiv Preprint arXiv:1703.08754, 2017.
[48] C. Qian, W. Sun, D.L. Hung, C. Qiu, M. Makaremi, S.G.H. Kumar, L. Wan, M. Ghoussoub, T.E. Wood, M. Xia, Catalytic CO 2 reduction by palladium-decorated silicon–hydride nanosheets, Nat. Catal. 2 (2019) 46–54.
[49] R. Zhao, X. Wei, H. Zhu, S. Li, H. Li, Edge stabilities and growth kinetics of graphene-like two dimensional monolayers composed with Group 15 elements, Phys. Chem. Chem. Phys. 24(2022)3348-3356.
[50] H. Yao, Z. Sun, L. Liang, X. Yan, Y. Wang, M. Yang, X. Hu, Z. Wang, Z. Li, M. Wang, Hybrid metasurface using graphene/graphitic carbon nitride heterojunctions for ultrasensitive terahertz biosensors with tunable energy band structure, Photon. Res. 11 (2023) 858–868.
[51] X. Zhang, Y. Tang, F. Zhang, C.S. Lee, A novel aluminum–graphite dual-ion battery, Adv. Energy Mater. 6 (2016) 1502588.
[52] M. Wang, X. Yang, W. Wang, Establishing a 3D aggregates database from X-ray CT scans of bulk concrete, Constr. Build. Mater. 315 (2022) 125740.
[53] R. Wang, H. Xie, X. Lai, J.-B. Liu, J. Li, G. Qiu, Visible light-enabled iron-catalyzed selenocyclization of N-methoxy-2-alkynylbenzamide, Mol. Catal. 515 (2021) 111881.
[54] P. Xu, J. Cao, C. Yin, L. Wang, L. Wu, Quantum chemical study on the adsorption of megazol drug on the pristine BC3 nanosheet, Supramol. Chem. 33 (2021) 63–69.
[55] H. Li, J. Tang, Y. Kang, H. Zhao, D. Fang, X. Fang, R. Chen, Z. Wei, Optical properties of quasi-type-II structure in GaAs/GaAsSb/GaAs coaxial single quantum-well nanowires, Appl. Phys. Lett. 113 (2018) 233104.
[56] T.H. Zhao, M.I. Khan, Y.M. Chu, Artificial neural networking (ANN) analysis for heat and entropy generation in flow of non-Newtonian fluid between two rotating disks, Math. Methods Appl. Sci. 46 (2021)3012-3030.
[57] M.A. Iqbal, Y. Wang, M.M. Miah, M.S. Osman, Study on date–Jimbo–Kashiwara–Miwa equation with conformable derivative dependent on time parameter to find the exact dynamic wave solutions, Fract. Fraction. 6 (2022) 4.
[58] H. Zeng, J. Zhao, A.-Q. Cheng, L. Zhang, Z. He, R.-S. Chen, Tuning electronic and optical properties of arsenene/C3N van der Waals heterostructure by vertical strain and external electric field, Nanotechnology 29 (2018) 075201.
[59] X. Zhou, W. Feng, S. Guan, B. Fu, W. Su, Y. Yao, Computational characterization of monolayer C3N: a two-dimensional nitrogen-graphene crystal, J. Mater. Res. 32 (2017) 2993–3001.
[60] M.W. Schmidt, K.K. Baldridge, J.A. Boatz, S.T. Elbert, M.S. Gordon, J.H. Jensen, S. Koseki, N. Matsunaga, K.A. Nguyen, S. Su, T.L. Windus, M. Dupuis, J.A. Montgomery Jr, General atomic and molecular electronic structure system, J. Comput. Chem. 14 (1993) 1347–1363.
[61] Y. Chu, T. Zhao, Concavity of the error function with respect to Hölder means, Math. Inequal. Appl. 19 (2016) 589–595.
[62] T.-H. Zhao, L. Shi, Y.-M. Chu, Convexity and concavity of the modified Bessel functions of the first kind with respect to Hölder means, in: Revista de la Real Academia de Ciencias Exactas, Físicas y Naturales. Serie A. Matemáticas, vol. 114, 2020, pp. 1–14.
[63] T.-H. Zhao, Z.-Y. He, Y.-M. Chu, On some refinements for inequalities involving zero-balanced hypergeometric function, AIMS Math. 5 (2020) 6479–6495.
[64] Y. Duan, Y. Liu, Z. Chen, D. Liu, E. Yu, X. Zhang, H. Fu, J. Fu, J. Zhang, H. Du, Amorphous molybdenum sulfide nanocatalysts simultaneously realizing efficient upgrading of residue and synergistic synthesis of 2D MoS 2 nanosheets/carbon hierarchical structures, Green Chem. 22 (2020) 44–53.
[65] T.-H. Zha, O. Castillo, H. Jahanshahi, A. Yusuf, M.O. Alassafi, F.E. Alsaadi, Y.-M. Chu, A fuzzy-based strategy to suppress the novel coronavirus (2019-NCOV) massive outbreak, Appl. Comput. Math. (2021) 160–176.
[66] A. Tkatchenko, R.A. DiStasio Jr, M. Head-Gordon, M. Scheffler, Dispersion-corrected Møller–Plesset second-order perturbation theory, J. Chem. Phys. 131 (2009) 094106.
[67] H. Cui, X. Zhang, J. Zhang, J. Tang, Adsorption behaviour of SF6 decomposed species onto Pd4-decorated single-walled CNT: a DFT study, Mol. Phys. 116 (2018) 1749–1755.
[68] T.-H. Zhao, M.-K. Wang, Y.-M. Chu, Concavity and bounds involving generalized elliptic integral of the first kind, J. Math. Inequal. 15 (2021) 701–724.
[69] M. Wang, C. Jiang, S. Zhang, X. Song, Y. Tang, H.-M. Cheng, Reversible calcium alloying enables a practical room-temperature rechargeable calcium-ion battery with a high discharge voltage, Nat. Chem. 10 (2018) 667–672.
[70] H. Zhu, J. Zhu, Z. Zhang, R. Zhao, Crossover from linear chains to a honeycomb network for the nucleation of hexagonal boron nitride grown on the Ni (111) surface, J. Phys. Chem. C 125 (2021) 26542–26551.
[71] M. Nazeer, F. Hussain, M.I. Khan, E.R. El-Zahar, Y.-M. Chu, M. Malik, Theoretical study of MHD electro-osmotically flow of third-grade fluid in micro channel, Appl. Math. Comput. 420 (2022) 126868.
[72] W. Ju, T. Li, X. Su, H. Li, X. Li, D. Ma, Au cluster adsorption on perfect and defective MoS 2 monolayers: structural and electronic properties, Phys. Chem. Chem. Phys. 19 (2017) 20735–20748.
[73] S. Rashid, E.I. Abouelmagd, A. Khalid, F.B. Farooq, Y.-M. Chu, Some recent developments on dynamical $\hbar$-discrete fractional type inequalities in the frame of nonsingular and nonlocal kernels, Fractals. 30 (2021)2240110.
[74] S. Rashid, S. Sultana, Y. Karaca, A. Khalid, Y.-M. Chu, Some further extensions considering discrete proportional fractional operators, Fractals 2240026 (2021).
[75] K. Karthikeyan, P. Karthikeyan, H.M. Baskonus, K. Venkatachalam, Y.M. Chu, Almost sectorial operators on Ψ-Hilfer derivative fractional impulsive integro-differential equations, Math. Methods Appl. Sci. 45(2021)8045-8059.
[76] H. Cui, C. Yan, P. Jia, W. Cao, Adsorption and sensing behaviors of SF6 decomposed species on Ni-doped C3N monolayer: a first-principles study, Appl. Surf. Sci. 512 (2020) 145759.
[77] X. Wang, Q. Li, H. Wang, Y. Gao, J. Hou, J. Shao, Anisotropic carrier mobility in single-and bi-layer C3N sheets, Phys. B Condens. Matter 537 (2018) 314–319.
[78] G. Henkelman, A. Arnaldsson, H. Jónsson, A fast and robust algorithm for Bader decomposition of charge density, Comput. Mater. Sci. 36 (2006) 354–360.
[79] X. Sun, J.-Y. Hwang, S. Xie, Density functional study of elemental mercury adsorption on surfactants, Fuel 90 (2011) 1061–1068.
[80] X. Li, L. Zhu, Q. Xue, X. Chang, C. Ling, W. Xing, Superior selective CO2 adsorption of C3N pores: GCMC and DFT simulations, ACS Appl. Mater. Interfaces 9 (2017) 31161–31169.
[81] A. Bafekry, M. Ghergherehchi, S. Farjami Shayesteh, F.M. Peeters, Adsorption of molecules on C3N nanosheet: a first-principles calculations, Chem. Phys. 526 (2019) 110442.
[82] J.-N. Zhang, L. Ma, M. Zhang, J.-M. Zhang, Effects of gas adsorption on electronic and optical properties of palladium-doped graphene: first-principles study, Phys. E. 118 (2020) 113879.
[83] S. Ma, D. Yuan, Y. Wang, Z. Jiao, Monolayer GeS as a potential candidate for NO 2 gas sensors and capturers, J. Mater. Chem. C 6 (2018) 8082–8091.